Seismic data analysis using local time-frequency decomposition[a]

[a]Published in Geophysical Prospecting, 61, 516525 (2013)

Yang Liu[*†], *Sergey Fomel*[†]

ABSTRACT

Many natural phenomena, including geologic events and geophysical data, are fundamentally nonstationary - exhibiting statistical variation that changes in space and time. Time-frequency characterization is useful for analyzing such data, seismic traces in particular.

We present a novel time-frequency decomposition, which aims at depicting the nonstationary character of seismic data. The proposed decomposition uses a Fourier basis to match the target signal using regularized least-squares inversion. The decomposition is invertible, which makes it suitable for analyzing nonstationary data. The proposed method can provide more flexible time-frequency representation than the classical S transform. Results of applying the method to both synthetic and field data examples demonstrate that the local time-frequency decomposition can characterize nonstationary variation of seismic data and be used in practical applications, such as seismic ground-roll noise attenuation and multicomponent data registration.

INTRODUCTION

Geological events and geophysical data often exhibit fundamentally nonstationary variations. Therefore, time-frequency characterization of seismic traces is useful for geophysical data analysis. A widely used method of time-frequency analysis is the short-time Fourier transform (STFT) (Allen, 1977). However, the window function limits the time-frequency resolution of STFT (Cohen, 1995). An alternative is the wavelet transform, which expands the signal in terms of wavelet functions that are localized in both time and frequency (Chakraborty and Okaya, 1995). However, because a wavelet family is built by restricting its frequency parameter to be inversely proportional to the scale, expansion coefficients in a wavelet frame may not provide precise enough estimates of the frequency content of waveforms, especially at high frequencies (Wang, 2007). Therefore, Sinha et al. (2005, 2009) developed a time-frequency continuous-wavelet transform (TFCWT) to describe time-frequency map more accurately than the conventional continuous-wavelet transform (CWT). The S transform (Stockwell et al., 1996) is another generalization of STFT, which extends CWT and

overcomes some of its disadvantages. Pinnegar and Mansinha (2003) developed a general version of the S transform by employing windows of arbitrary and varying shape. The clarity of the S transform is worse than the Wigner-Ville distribution function (Wigner, 1932), which achieves a higher resolution but is seldom used in practice because of its well-known drawbacks, such as interference and aliasing. For this reason, Li and Zheng (2008) provided a smoothed Wigner-Wille distribution (SWVD) to reduce the interference caused by the cross-term interference. The matching pursuit method is yet another approach to representing the time-frequency signature (Liu and Marfurt, 2007; Wang, 2007, 2010). Matching pursuit involves several parameters and is a relatively expensive method. There are some other approaches to spectral decomposition. Castagna and Sun (2006) compare several different spectral-decomposition methods.

Liu et al. (2009, 2011) recently proposed a new method of time-varying frequency characterization of nonstationary seismic signals that is based on regularized least-squares inversion. In this paper, we expand the method of Liu et al. (2011) by designing an invertible nonstationary time-frequency decomposition — *local time-frequency (LTF) decomposition* and its extensions — *local time-frequency-wavenumber (LTFK)* and *local space-frequency-wavenumber (LXFK) decompositions*. The key idea is to minimize the error between the input signal and all its Fourier components simultaneously using regularized nonstationary regression (Fomel, 2009) with control on time resolution. This approach is generic, in the sense that it is possible to combine other basis functions, eg., fractional splines, with regularization (Herrmann, 2001). Although there is an iterative inversion inside the algorithm, one can use LTF decomposition as an invertible "black box" transform from time to time-frequency, similar in properties to the S transform. The proposed decompositions can provide local time-frequency or space-wavenumber representations for common seismic data-processing tasks. We test the new method and compare it with the S transform by using a classical benchmark signal with two crossing chirps. The proposed LTF decomposition appears to provide higher resolution in both time and frequency when an appropriate parameters of the shaping regularization operator (Fomel, 2007b) are used to constrain the time resolution. Examples of ground-roll attenuation and multicomponent image registration demonstrate that the method can be effective in practical applications.

THEORY

Local time-frequency (LTF) decomposition

The Fourier series is by definition an expansion of a function in terms of a sum of sines and cosines. Letting a causal signal, $f(x)$, be in range of $[0, L]$, the Fourier series

of the signal is given by

$$f(x) = \frac{a_0}{2} + \sum_{n=1}^{\infty} \left[a_n \cos\left(\frac{2\pi n x}{L}\right) + b_n \sin\left(\frac{2\pi n x}{L}\right) \right] . \tag{1}$$

The notion of a Fourier series can also be extended to complex coefficients as follows:

$$f(x) = \sum_{n=-\infty}^{\infty} A_n \Psi_n(x) , \tag{2}$$

where A_n are the Fourier coefficients and $\Psi_n(x) = e^{i(2\pi n x/L)}$.

Nonstationary regression allows the coefficients A_n to change with x. In the linear notation, $A_n(x)$ can be obtained by solving the least-squares minimization problem

$$\min_{A_n} \|f(x) - \sum_n A_n(x)\Psi_n(x)\|_2^2 . \tag{3}$$

The minimization problem is ill posed because there are a lot more unknown variables than constraints. Our solution is to include additional constraints in the form of regularization, which limits the allowed variability of the estimated coefficients (Fomel, 2009). Tikhonov's regularization (Tikhonov, 1963) can modify the objective function to

$$\widetilde{A_n}(x) = \arg\min_{A_n} \|f(x) - \sum_n A_n(x)\Psi_n(x)\|_2^2 + \epsilon^2 \sum_n \|\mathbf{D}[A_n(x)]\|_2^2 , \tag{4}$$

where $\mathbf{D}$ is the *regularization* operator and ϵ is a scaling parameter. One can define $\mathbf{D}$, for example, as a gradient operator that penalizes roughness of $A_n(x)$.

We use shaping regularization (Fomel, 2007b) instead of Tikhonov's regularization to constrain the least-squares inversion. Shaping is a general method for imposing constraints by explicit mapping the estimated model to the desired model, eg., smooth model. Instead of trying to find and specify an appropriate regularization operator, the user of the shaping-regularization algorithm specifies a shaping operator, which is often easier to design.

The absolute value of time-varying coefficients $|A_n(x)|$ provides a time-frequency representation, and equation 2 provides the inverse calculation. In the discrete form, a range of frequencies can be decided by the Nyquist frequency (Cohen, 1995) or by the user's assignment. In a somewhat different approach, Liu et al. (2009) minimized the error between the input signal and each frequency component independently. Their algorithm and the proposed algorithm are equivalent when the decomposition is stationary (or using a very large shaping radius), because they both reduce to the regular Fourier transform. In the case of nonstationarity, their approach does not guarantee invertability, because it processes each frequency independently.

Local t-f-k (LTFK) and local x-f-k (LXFK) decompositions

Askari and Siahkoohi (2008) proposed t-f-k and x-f-k transforms that are based on the S transform. We define analogous LTFK and LXFK decompositions by using the LTF decomposition. The new decompositions can be used to design general time-varying or space-varying FK filters. The key steps of the algorithm are illustrated schematically in Figure 1.

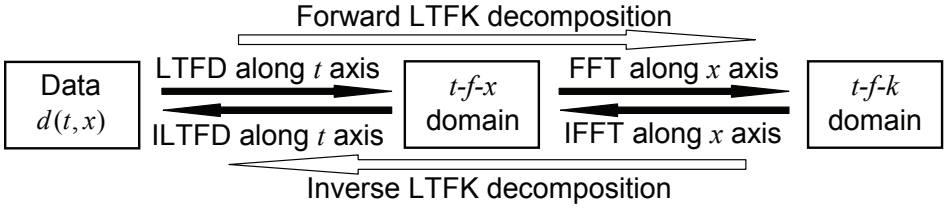

a

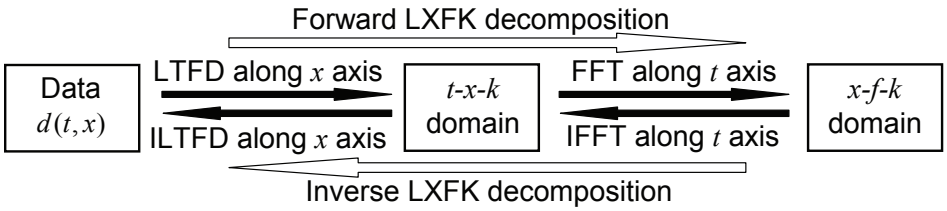

b

Figure 1: Schematic illustration of LTFK decomposition (a) and LXFK decomposition (b) by using the LTF decomposition.

Example of Time-frequency Characterization

A simple 1-D example is shown in Figure 2. The input signal includes two crossing chirp signals and displays nonstationary characteristics (Figure 2a). We applied the LTF decomposition to obtain a time-frequency distribution. Figure 3a shows that the proposed method recovers the linear frequency trend with high resolution in both time and frequency. In comparison, the S transform has high resolution near low frequencies but loses resolution at high frequencies (Figure 2b). Figure 3b displays the LTF decomposition using a different smoothing parameter (14 points) to demonstrate adjustable time-frequency characteristics of the LTF decomposition.

APPLICATION TO GROUND-ROLL ATTENUATION

Seismic data always consist of signal and noise components. The time-frequency denoising algorithm is an effective method for handling noise problems (Elboth et al., 2010). Ground roll is the main type of coherent noise in land seismic surveys and

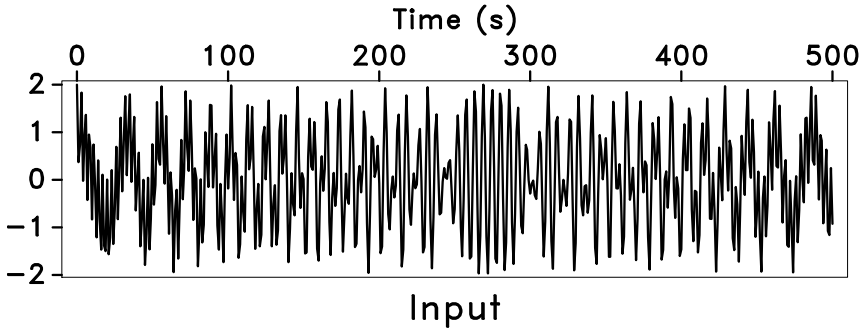

a

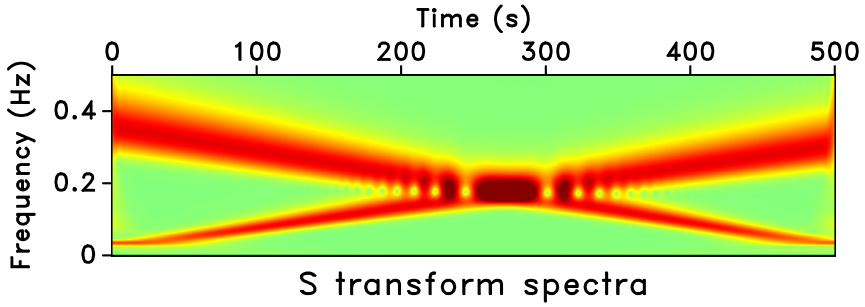

b

Figure 2: Synthetic signal with two crossing chirps (a) and time-frequency spectra from S transform (b).

is characterized by low frequencies and high amplitudes. Current processing techniques for attenuating ground roll include frequency filtering, FK filtering (Yilmaz, 2001), radon transform (Liu and Marfurt, 2004), wavelet transform (Deighan and Watts, 1997), and the curvelet transform (Yarham and Herrmann, 2008). Askari and Siahkoohi (2008) applied the S transform to ground-roll attenuation. Here, we propose a similar strategy, except that we are applying the proposed local time-frequency decomposition instead of the S transform.

We applied our methods to a land shot gather contaminated by nearly radial ground roll (Figure 4a). All time-domain images are obtained after automatic gain control (AGC). We applied the forward LTF decomposition to each trace to generate a time-frequency cube (Figure 5a). Note that the ground roll is distributed at localized time-space (left-down section of Figure 5a) and time-frequency (right-down section of Figure 5a) positions. The LTF decomposition is flexible, due to its adjustable time-frequency resolution. Therefore, we designed a simple muting filter to remove the noise components localized in both frequency and space (Figure 5b). The inverse LTF decomposition brings the separated signal back to the original domain (Figure 4). Figure 4c shows the difference between raw data (Figure 4a) and denoised result using LTF decomposition (Figure 4b). It is possible to design more complicated but more powerful masks. Without a time-space mask, our method of simply muting selected frequencies would reduce to band-pass filtering.

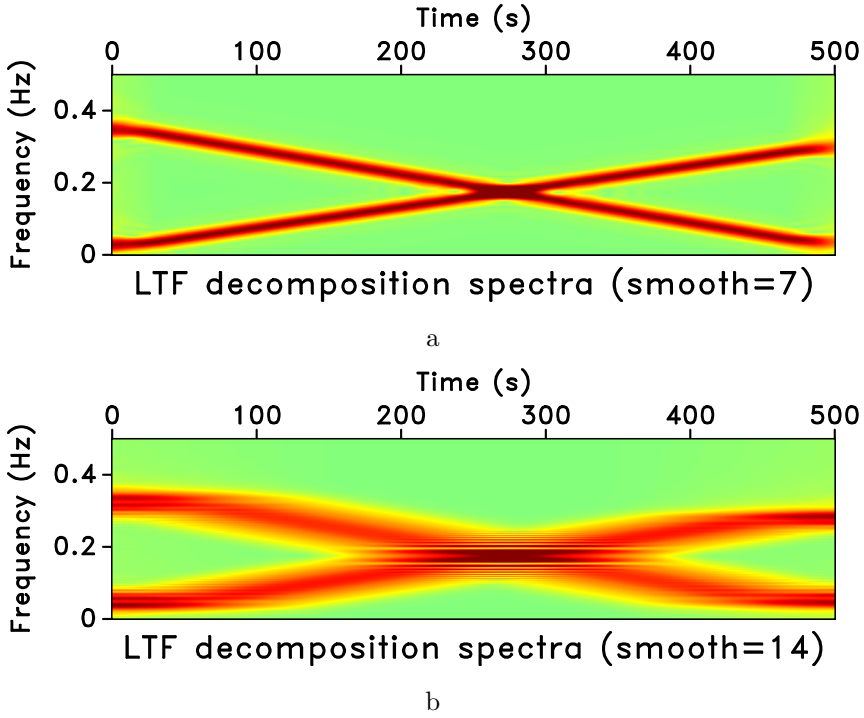

Figure 3: Time-frequency spectra from LTF decomposition with different sizes of the smoothing radius. Smoothing radius of 7 points (a) and smoothing radius of 14 points (b).

The LTFK and LXFK decompositions generate data in different domains (Figure 6a and 7a), which show the trend of ground-roll noise in the frequency-wavenumber sections. Simple frequency-wavenumber masks (Figure 6b and 7b) can eliminate ground-roll noise in the decomposition domains. The recovered signals using the inverse LTFK and LXFK decompositions produce similar results (Figure 8a and 8b, respectively). Furthermore, different decompositions can be cascaded to improve their denoising abilities. For comparison, we used a simple high-pass filter. Figure 9a shows that the high-pass filter fails in removing noise, a larger filter window can damage the seismic signal. Another choice is FK filtering (Figure 9b), which cannot remove the low-frequency part of ground-roll noise. The result is similar to that of the LXFK decomposition (Figure 8b), but the proposed method tends to remove more noise than the standard FK filter (especially near location of time 2.7s and offset 1.2km in Figure 8b and 9b) because of the decomposition's locality and its more flexible design. Radial trace (RT) transform is another approach to deal with ground-roll noise, which is a simple geometric re-mapping method of a seismic trace gather. Idealized ground roll is transformed to small temporal frequency by the RT transform and can be eliminated by applying the RT transform, followed by high-pass filtering and the inverse RT transform (Claerbout, 1983; Henley, 1999). Figure 10a shows that the RT transform performs better than the high-pass filter or the FK filter. However, it still has trouble separating signal and noise near the source. Figure 10b shows the

denoised result after cascading the proposed LXFK and LTF decompositions, which achieved the best result in this case (especially at locations around the bottom left corner).

APPLICATION TO MULTICOMPONENT DATA REGISTRATION

Multicomponent seismic data provide additional information about subsurface physical characteristics (Stewart et al., 2003). Joint interpretation of multiple image components depends on our ability to identify and register reflection events from similar reflectors. Fomel and Backus (2003) and Fomel et al. (2005) proposed a multistep approach for registering PP and PS images, and identified spectral differences between PP and PS images as a major problem that prevents an easy automatic registration. The new LTF decomposition can provide a natural domain for nonstationary spectral balancing of multicomponent images.

Figure 11a and b show seismic images from compressional (PP) and shear (SS) reflections obtained by processing a land nine-component survey (Fomel, 2007a). One can use "image warping" (Wolberg, 1990) to squeeze the SS image to PP reflection time and make the two images display in the same coordinate system. Using initial interpretation and well-log analysis, we identified three individual correlation "nails" in the terminology of DeAngelo et al. (2003). Fitting a straight line through the nails suggests a constant initial V_P/V_S ratio (Figure 12). For illustration of spectral balancing, we select the 300th trace in the PP and SS images and then warp (squeeze) SS time to PP time by using the initial V_P/V_S ratio. The corresponding local time-frequency spectra are shown in Figures 13a and b. The SS-trace frequency appears higher in the shallow part of the image because of a relatively low S-wave velocity but lower in the deeper part of the image because of the apparently stronger attenuation of shear waves. Spectral balancing essentially smoothes the high-frequency image to match the low-frequency image. The LTF decompositions provide a nonstationary domain for time-varying spectral balancing. Our spectral balancing works as follows. For each time slice in LTF domains, we use three steps:

1. Match the PP and SS spectra by least-squares fitting with Ricker spectra

$$R_i(f) = A_i^2 \frac{f^2}{f_i^2}\, e^{-f^2/f_i^2} \;, \tag{5}$$

   where f is frequency axis and get the dominant frequencies f_1 and f_2 ($f_2 > f_1$) and the corresponding amplitudes A_1 and A_2.

2. Use the estimated Ricker parameters to design a matching Gaussian filter

$$G(f) = \frac{A_1 f_2^2}{A_2 f_1^2}\, e^{f^2(1/f_2^2 - 1/f_1^2)} \;. \tag{6}$$

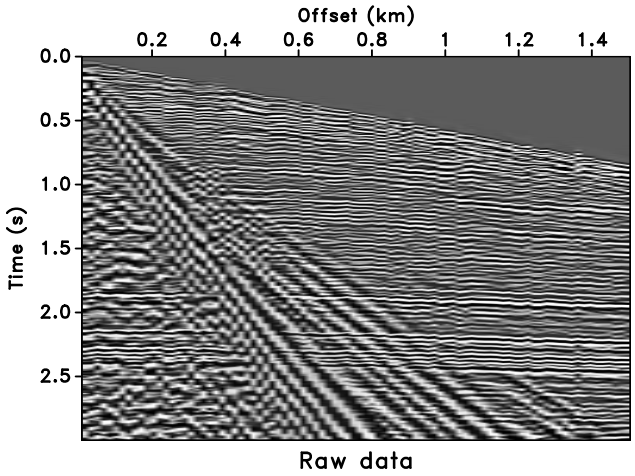

a

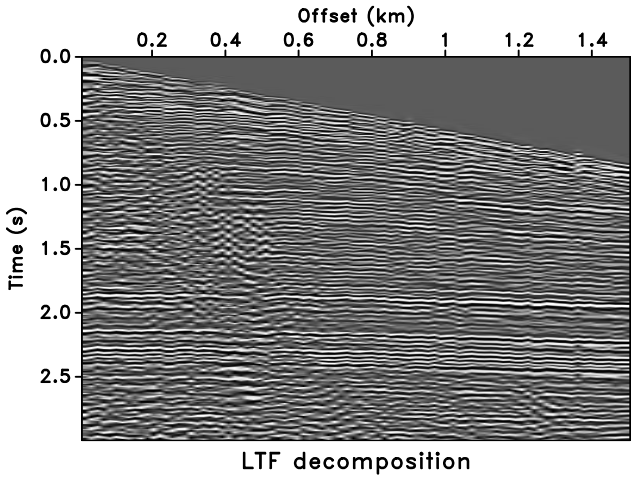

b

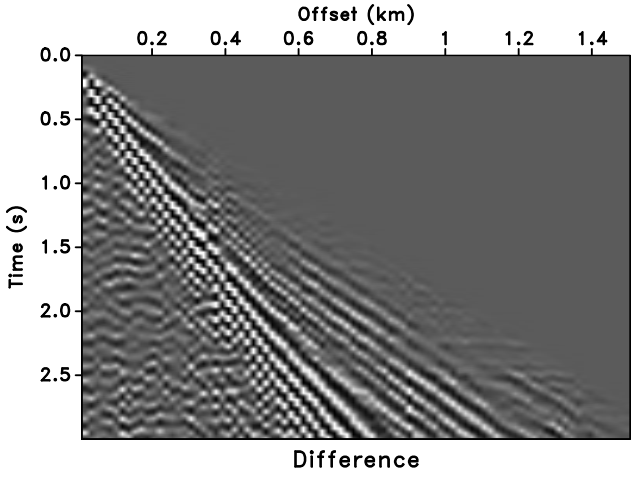

c

Figure 4: Field land data (a), denoised result using LTF decomposition (b), and difference between raw data (Figure 4a) and denoised result using LTF decomposition (Figure 4b) (c).

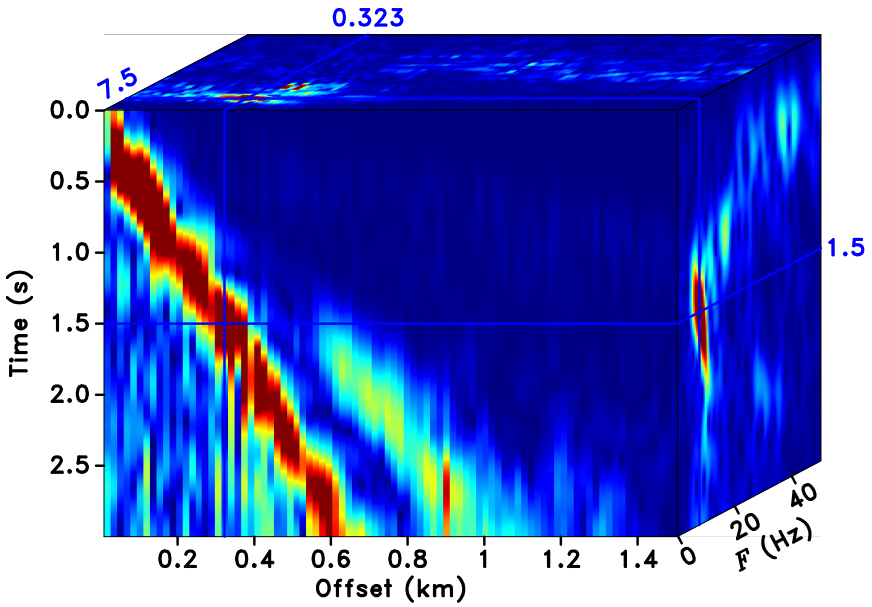

a

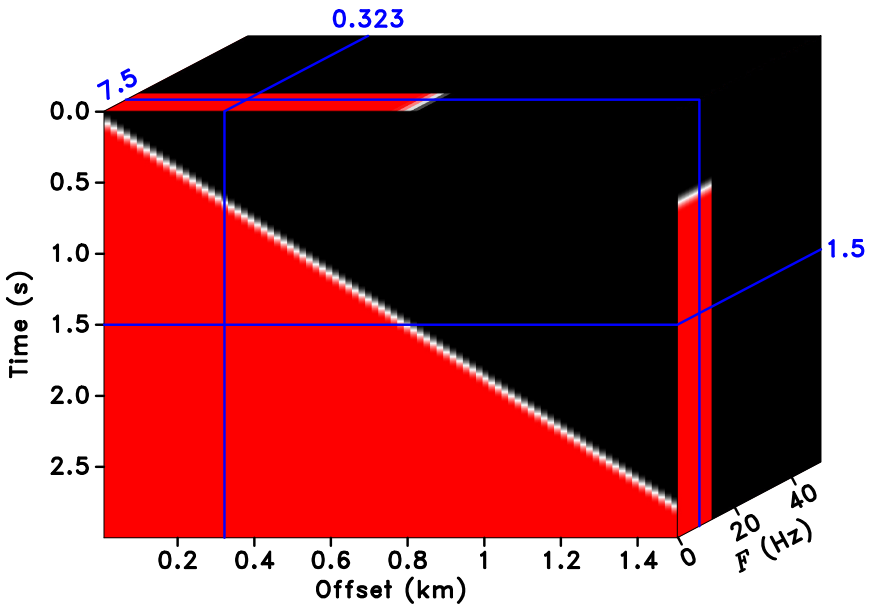

b

Figure 5: Local T-X-F spectra (a) and filter mask in T-X-F domain (b).

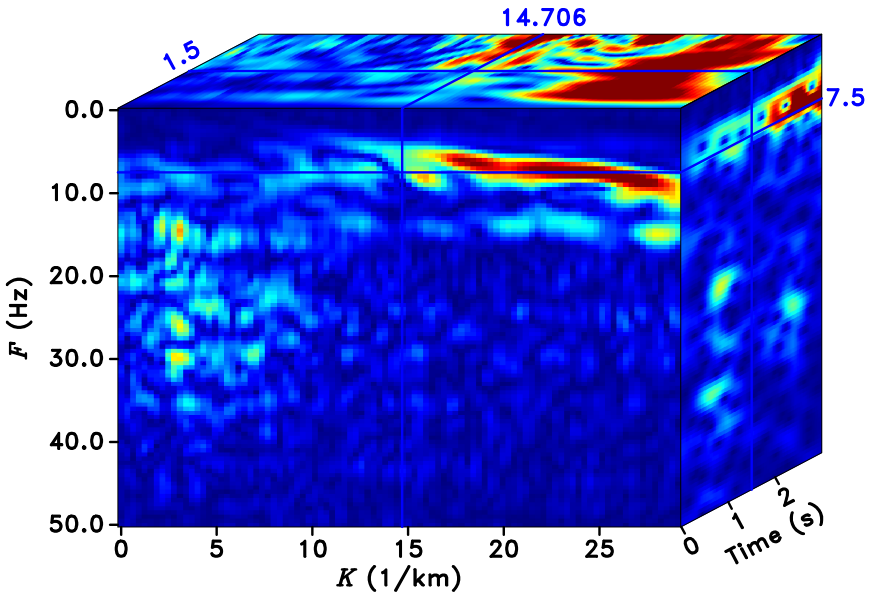

a

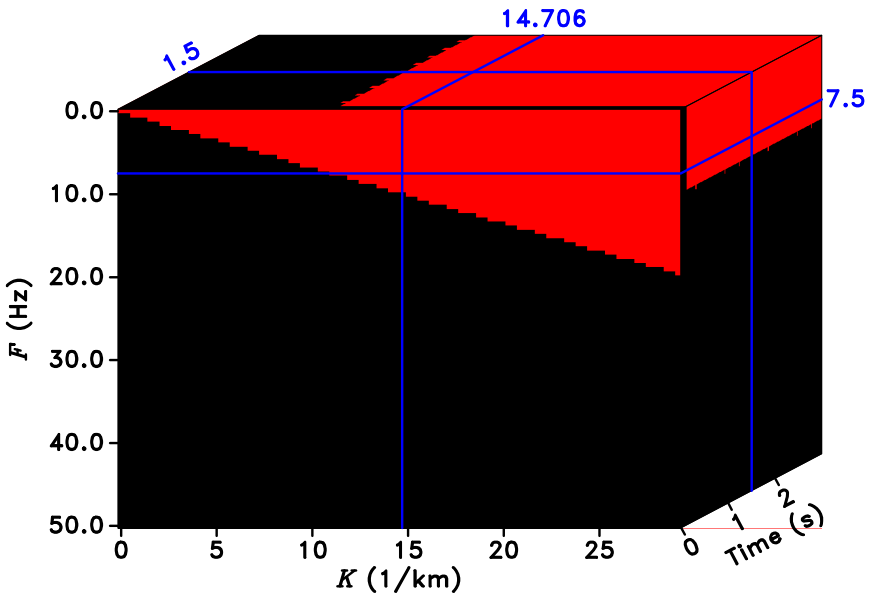

b

Figure 6: Local F-K-T spectra (a) and filter mask in F-K-T domain (b).

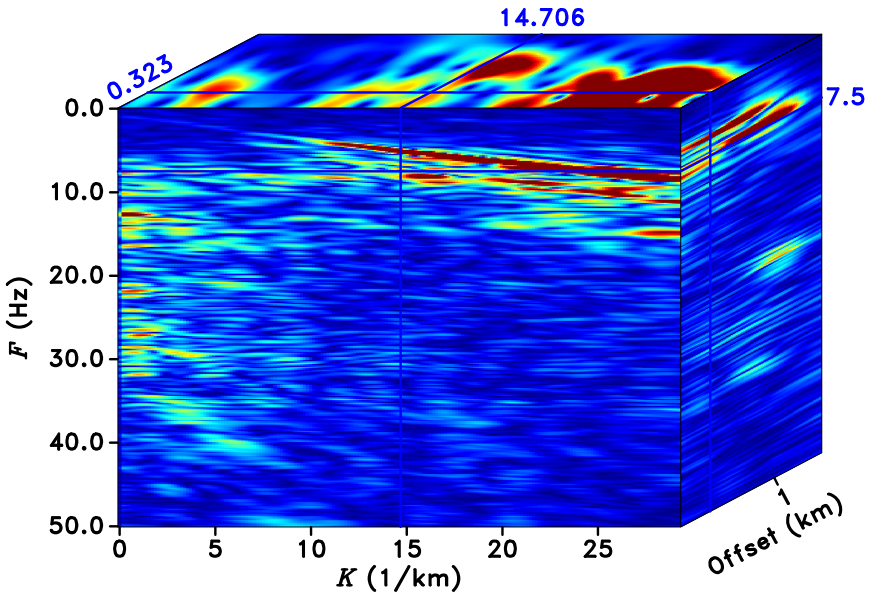

a

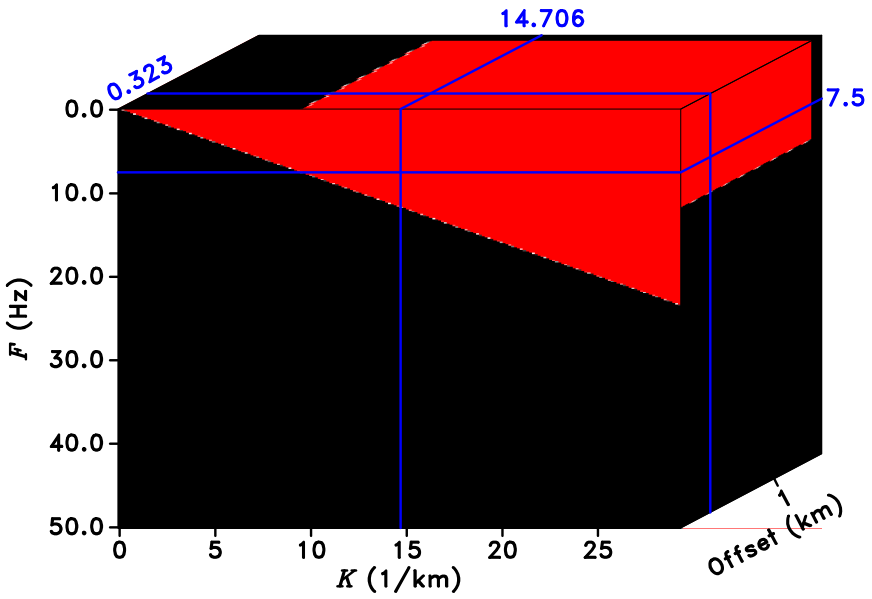

b

Figure 7: Local F-K-X spectra (a) and filter mask in F-K-X domain (b).

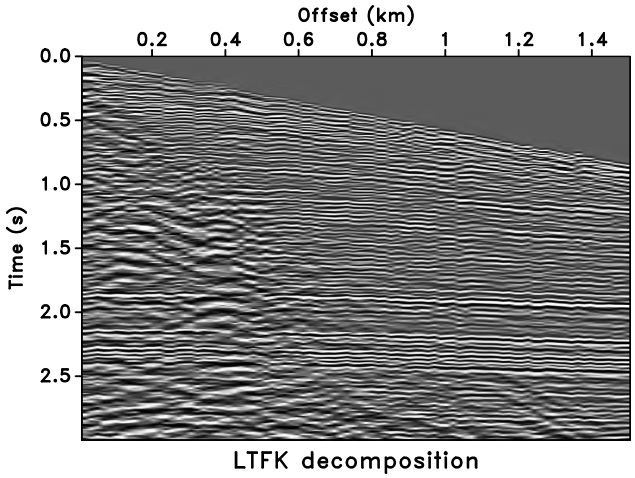

a

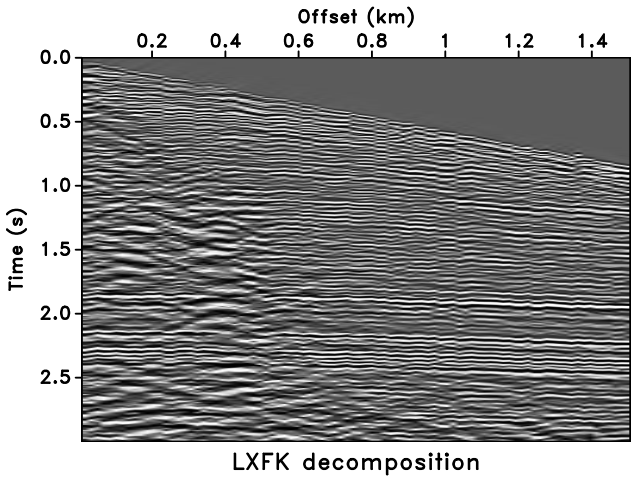

b

Figure 8: Denoised results using different local decompositions. LTFK decomposition (a) and LXFK decomposition (b).

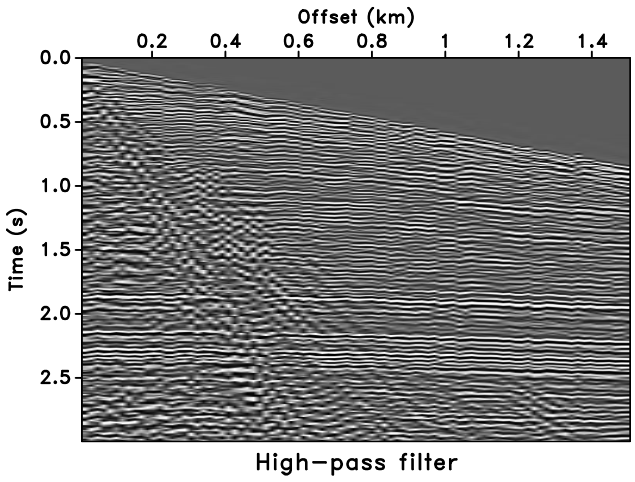

a

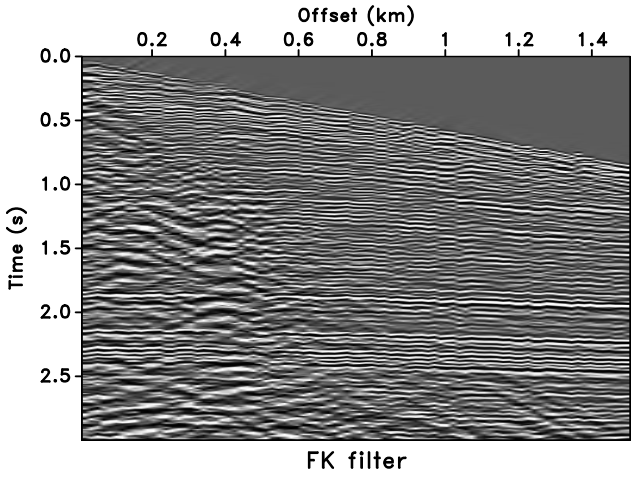

b

Figure 9: Denoised data using different methods (shown for comparison). High-pass filter (a) and FK filter (b).

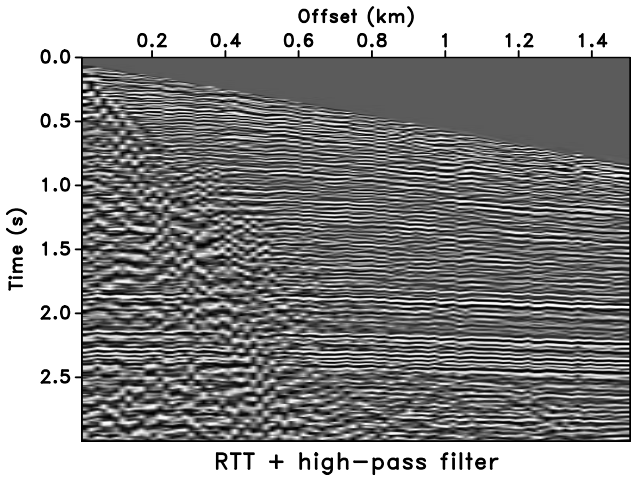

a

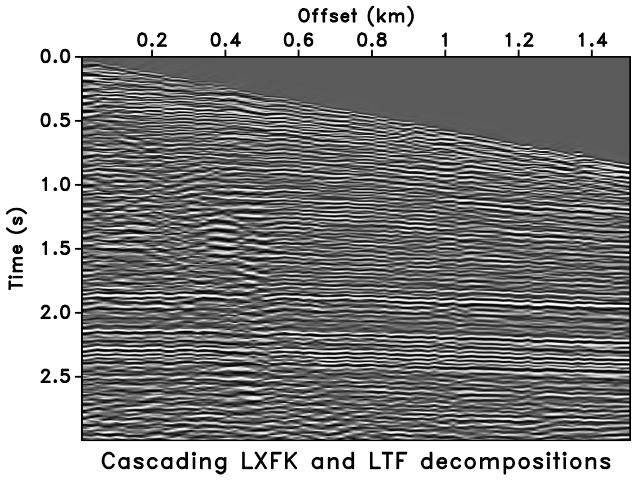

b

Figure 10: Denoised result by using RT transform with high-pass filter (a) and cascading LXFK and LTF decompositions (b).

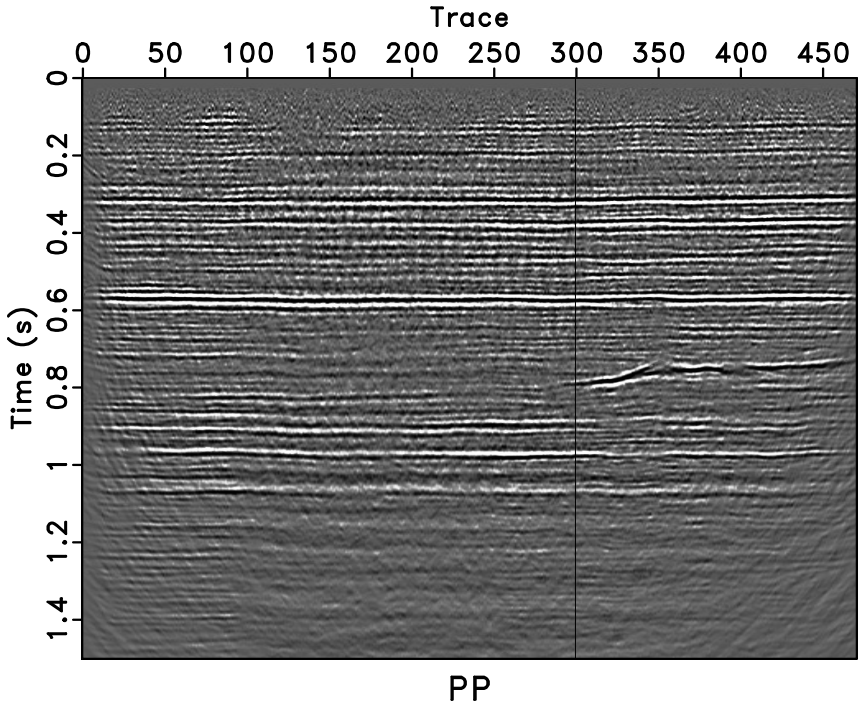

a

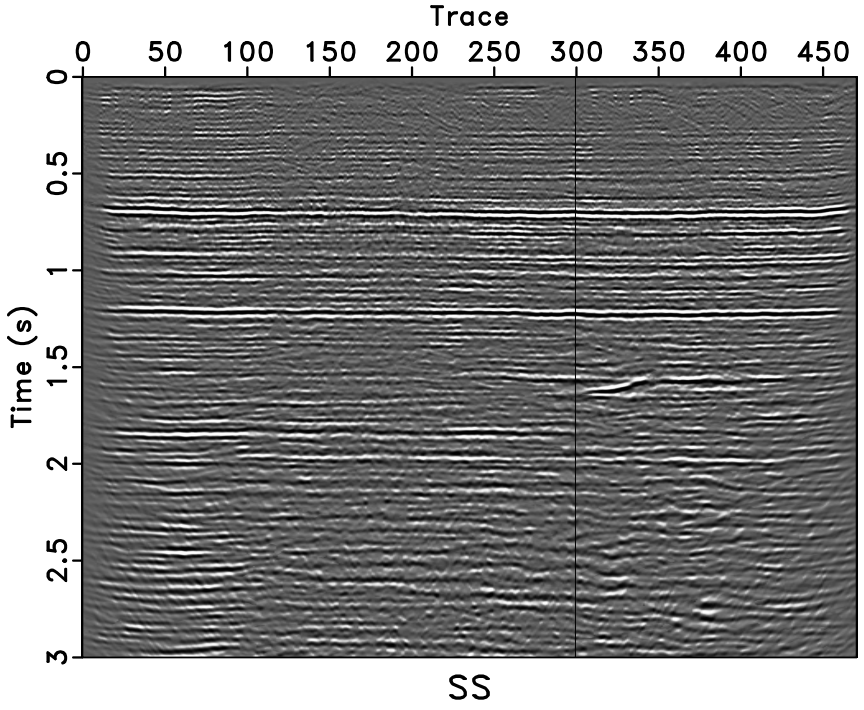

b

Figure 11: PP (a) and SS (b) images from a nine-component land survey.

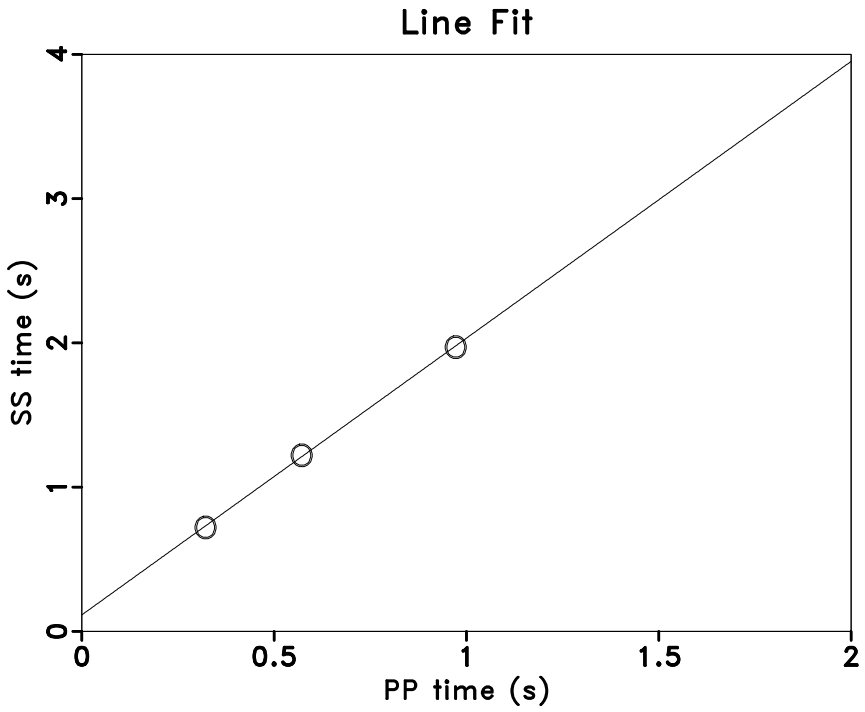

Figure 12: Three "nails" for PP and SS time correlation identified by initial image interpretation and fitted to a straight line.

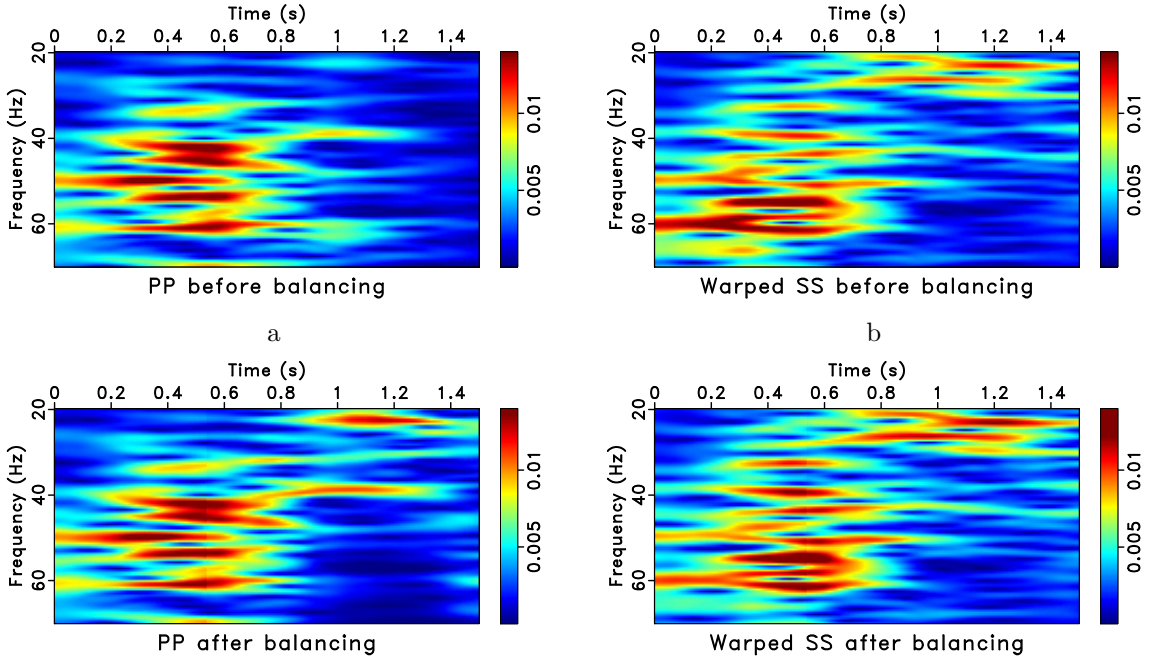

Figure 13: Time-frequency spectra in LTF decomposition domain. PP before balancing (a), SS after initial warping (b), PP after balancing (c), and warped SS after balancing (d).

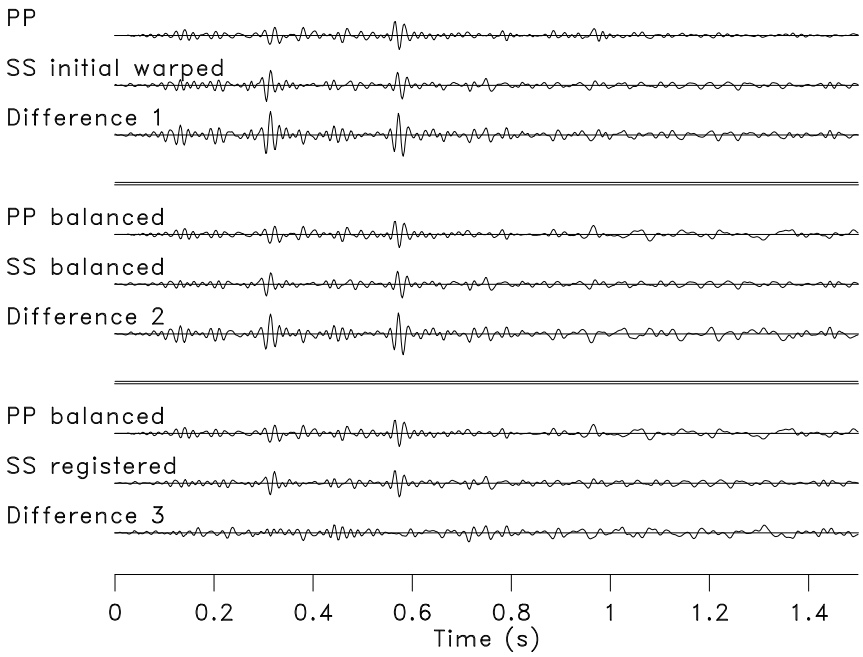

Figure 14: Three stages for PP and SS registration. Initial warping (top), nonstationary spectral balancing (middle), and final registration after warping scan (bottom).

3. Shrink the high-frequency spectra to match the low-frequency spectra by applying the Gaussian filter.

The LTF spectra of PP and warped SS trace after nonstationary spectral balancing are shown in Figure 13c and d, respectively, which shows a reasonable similarity between the PP and SS traces for both shallow and deep parts. The inverse LTF decomposition reconstructs balanced PP and SS waveforms in the time domain. Figure 14 displays PP trace, SS trace, and the difference between the two traces in time domain, which are compared for three stages of automatic data registration (Fomel et al., 2005). Residual γ scan is an algorithm for rapid scanning of the field of possible registrations. After applying residual γ scan to update V_P/V_S ratio, the difference between balanced PP and registered SS traces is substantially reduced compared to the initial registration. The final registration result is visualized in Figure 15, which shows interleaved traces from PP and SS images before and after registration. The alignment of main seismic events (especially those at locations "A" and "B") is an indication of successful registration.

CONCLUSION

We have introduced a new time-frequency decomposition that uses regularized nonstationary regression with Fourier bases to represent the time-frequency variation of nonstationary signals. The decomposition is invertible and provides an explicit control

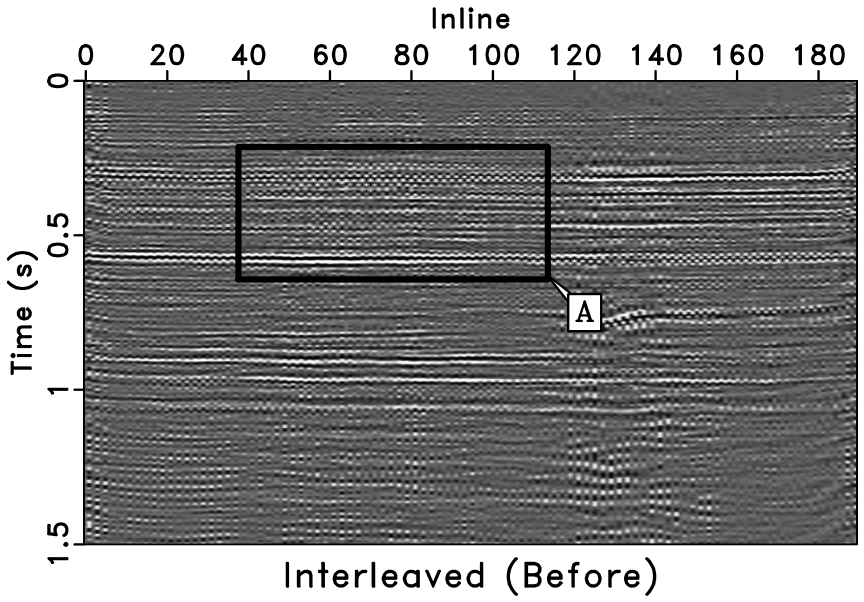

a

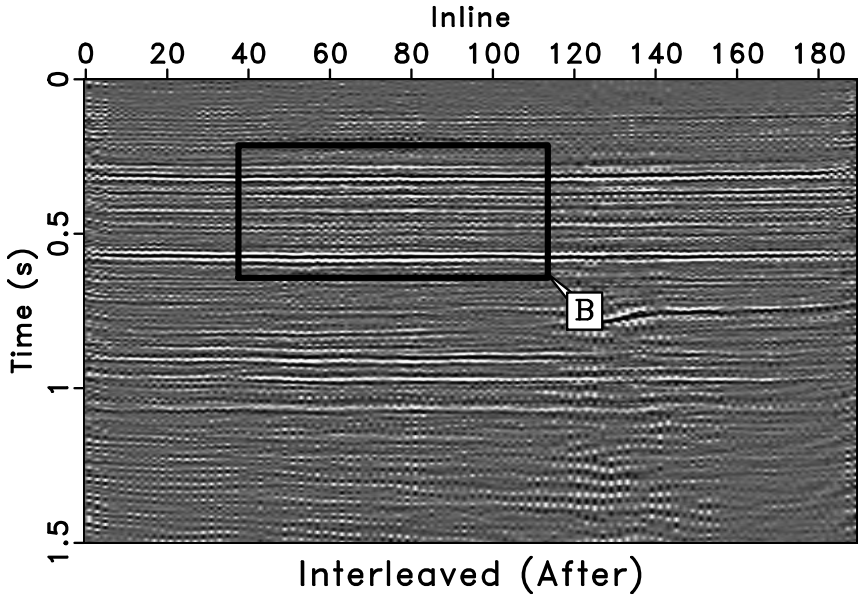

b

Figure 15: Interleaved traces from PP and SS images before (a) and after (b) multi-component registration.

on the time and frequency resolution of the time-frequency representation. Experiments with synthetic and field data show that the proposed local time-frequency decomposition can depict nonstationary variation and provide a useful domain for practical applications, such as ground-roll noise attenuation and multicomponent image registration.

ACKNOWLEDGMENTS

We thank Guochang Liu and Mirko van der Baan for stimulating discussions. We thank Partha Routh, one anonymous associate editor, and one anonymous reviewer for helpful suggestions, which improved the quality of the paper. This work is supported in part by National Natural Science Foundation of China (Grant No. 41004041) and 973 Programme of China (Grant No. 2009CB219301). This publication was authorized by the Director, Bureau of Economic Geology, The University of Texas at Austin.

REFERENCES

Allen, J. B., 1977, Short term spectral analysis, synthetic and modification by discrete Fourier transform: IEEE Transactions on Acoustic, Speech, Signal Processing, **25**, 235–238.

Askari, R., and H. R. Siahkoohi, 2008, Ground roll attenuation using the S and x-f-k transforms: Geophysical Prospecting, **56**, 105–114.

Castagna, J. P., and S. Sun, 2006, Comparison of spectral decomposition methods: First break, **24**, 75–79.

Chakraborty, A., and D. Okaya, 1995, Frequency-time decomposition of seismic data using wavelet-based method: Geophysics, **60**, 1906–1916.

Claerbout, J. F., 1983, Ground roll and radial traces: Stanford Exploration Project, **SEP-35**, 43–54.

Cohen, L., 1995, Time-frequency analysis: Prentice Hall, Inc.

DeAngelo, M. V., M. Backus, B. A. Hardage, P. Murray, and S. Knapp, 2003, Depth registration of P-wave and C-wave seismic data for shallow marine sediment characterization, Gulf of Mexico: The Leading Edge, **22**, 96–105.

Deighan, A. J., and D. R. Watts, 1997, Ground-roll suppression using the wavelet transform: Geophysics, **62**, 1896–1903.

Elboth, T., I. V. Presterud, and D. Hermansen, 2010, Time-frequency seismic data de-noising: Geophysical Prospecting, **58**, 441–453.

Fomel, S., 2007a, Local seismic attributes: Geophysics, **72**, A29–A33.

———, 2007b, Shaping regularization in geophysical-estimation problems: Geophysics, **72**, R29–R36.

———, 2009, Adaptive multiple subtraction using regularized nonstationary regression: Geophysics, **74**, V25–V33.

Fomel, S., and M. Backus, 2003, Multicomponent seismic data registration by least squares: 73rd Annual International Meeting, SEG, Expanded Abstracts, 781–784.

Fomel, S., M. Backus, K. Fouad, B. Hardage, and G. Winters, 2005, A multistep approach to multicomponent seismic image registration with application to a West Texas carbonate reservoir study: 75th Annual International Meeting, SEG, Expanded Abstracts, 1018–1021.

Henley, D., 1999, The radial trace transform: An effective domain for coherent noise attenuation and wavefield separation: 69nd Annual International Meeting, SEG, Expanded Abstracts, 1204–1207.

Herrmann, F. J., 2001, Fractional spline matching pursuit: A quantitative tool for seismic stratigraphy: 71st Annual International Meeting, SEG, Expanded Abstracts, 1965–1968.

Li, Y., and X. Zheng, 2008, Spectral decomposition using wigner-ville distribution with applications to carbonate reservoir characterization: The Leading Edge, **27**, 1050–1057.

Liu, G., S. Fomel, and X. Chen, 2009, Time-frequency characterization of seismic data using local attributes: 79nd Annual International Meeting, SEG, Expanded Abstracts, 1825–1829.

———, 2011, Time-frequency characterization of seismic data using local attributes: Geophysics, **76**, P23–P34.

Liu, J., and K. J. Marfurt, 2004, 3-d high resolution radon transforms applied to ground roll suppression in orthogonal seismic surveys: 74th Annual International Meeting, SEG, Expanded Abstracts, 2144–2147.

———, 2007, Instantaneous spectral attributes to detect channels: Geophysics, **72**, P23–P31.

Pinnegar, C., and L. Mansinha, 2003, The S-transform with windows of arbitrary and varying shape: Geophysics, **68**, 381–385.

Sinha, S., P. S. Routh, and P. Anno, 2009, Instantaneous spectral attributes using scales in continuous-wavelet transform: Geophysics, **74**, WA137–WA142.

Sinha, S., P. S. Routh, P. Anno, and J. P. Castagna, 2005, Spectral decomposition of seismic data with continuous-wavelet transform: Geophysics, **70**, P19–P25.

Stewart, R. R., J. Gaiser, R. J. Brown, and D. C. Lawton, 2003, Converted-wave seismic exploration: Applications: Geophysics, **68**, 40–57.

Stockwell, R. G., L. Mansinha, and R. P. Lowe, 1996, Localization of the complex spectrum: the S transform: IEEE Transactions on Signal Processing, **44**, 998–1001.

Tikhonov, A. N., 1963, Solution of incorrectly formulated problems and the regularization method: Soviet Mathematics – Doklady.

Wang, Y., 2007, Seismic time-frequency spectral decomposition by matching pursuit: Geophysics, **72**, V13–V20.

———, 2010, Multichannel matching pursuit for seismic trace decomposition: Geophysics, **75**, V61–V66.

Wigner, W., 1932, On the quantum correction for thermodynamic equilibrium: Physical Review, **40**, 749–759.

Wolberg, G., 1990, Digital image warping: IEEE Computer Society.

Yarham, C., and F. J. Herrmann, 2008, Bayesian ground-roll separation by curvelet-

domain sparsity promotion: 78th Annual International Meeting, SEG, Expanded Abstracts, 2576–2580.

Yilmaz, Ö., 2001, Seismic data analysis: Processing, inversion and interpretation of seismic data: Society of Exploration Geophysics.